Late Gadolinium Enhancement Imaging

15

Rebecca E. Thornhill and Elena Peña

Abstract

Late gadolinium enhancement cardiac magnetic resonance (LGE-CMR) has become a powerful and indispensable tool for the characterization of myocardial fibrosis and scar. LGE images can be acquired using any one of a number of fast T_1-weighted gradient echo sequences, approximately 10–20 min post-injection of contrast media. As such, LGE imaging is a simple technique that is an integral part of most clinical CMR protocols. In this chapter, we explore the fundamental principles underpinning the technique, beginning with a discussion of gadolinium contrast kinetics in both normal and damaged myocardium. Next, we describe the underlying basis for LGE imaging: nulling the MRI signal associated with normal myocardium, such that fibrotic or scarred tissue becomes conspicuously bright on T_1-weighted images. The chapter continues by providing a brief history of the evolution of LGE pulse sequence development, highlighting many crucial innovations along the way. Finally, we explore a variety of clinical applications of LGE, including its role in the characterization of infarct scar, in multiple cardiomyopathies, and in the rule-out of infectious or infiltrative disease. Common approaches for quantification and characterization of LGE images are also described. While by no means exhaustive, the goal of this chapter is to provide the cardiovascular imager with an understanding of the basic principles of LGE as well as an appreciation for the versatility and clinical utility of the technique.

Keywords

Late gadolinium enhancement • Myocardial viability • Myocardial infarction • Ischemic heart disease • Dilated cardiomyopathy • Hypertrophic cardiomyopathy • Arrhythmogenic right ventricular cardiomyopathy • Cardiac sarcoidosis • Myocarditis • Cardiac amyloidosis

R.E. Thornhill, PhD (✉)
Department of Radiology, University of Ottawa,
Ottawa, ON, Canada

Clinical Epidemiology Program, Ottawa Hospital Research Institute, Ottawa, ON, Canada

Department Medical Imaging c/o Laura Lang, The Ottawa Hospital, Civic Campus,
1053 Carling Ave, Ottawa, ON K1Y 4E9, Canada
e-mail: rthornhill@toh.on.ca

E. Peña, MD
Department of Medical Imaging, The Ottawa Hospital,
Ottawa, ON, Canada

Department of Radiology, University of Ottawa,
Ottawa, ON, Canada

M.A. Syed et al. (eds.), *Basic Principles of Cardiovascular MRI: Physics and Imaging Technique*,
DOI 10.1007/978-3-319-22141-0_15

Introduction

Late gadolinium enhancement (LGE) has become the gold standard in vivo imaging test for assessing the presence and extent of a wide range of myocardial abnormalities, most commonly infarct scar but also fibrosis of nonischemic disease and inflammatory and other infiltrative materials. With LGE, image acquisition occurs at a set delay (10–15 min) following the intravenous injection of gadolinium-based contrast media, in order to capture a 'snapshot' of the extravascular-extracellular distribution of contrast. The signal from normal (non-fibrotic) myocardium is deliberately "nulled" in LGE imaging, such that areas of accumulated contrast will appear bright. While clinical use of LGE-CMR in cardiovascular practice has expanded considerably in the last decade, the fundamental principle of exploiting the differential distribution of gadolinium-based contrast media in infarcted vs. normal myocardium was established in the mid-1980s [1–5]. In the approximately 30 years since, the LGE technique has undergone an impressive series of improvements, evolving from the low contrast-to-noise (CNR), single-slice, ungated spin-echo implementation of the early 1980s to the current state-of-the-art 3D pulse-sequences that are pushing towards resolving left atrial scar. In this chapter, we will discuss many of the key technical developments along this 30-year path, as well as illustrating how these advancements have enabled an expanding variety of clinical applications.

The Fundamental Principles of Late Gadolinium Enhancement

Compared with other CMR procedures, such as stress imaging, LGE is relatively straightforward. For most indications, LGE can be insinuated into the protocol approximately 12–14 min post-contrast injection and requires little more than 5 min to obtain full cardiac coverage in multiple views. In general, the left ventricle (LV) is best covered by acquiring contiguous short-axis views, from the apex to the level of the mitral valve with standard long axis views (horizontal long axis (HLA) or four-chamber, vertical long axis (VLA) or two-chamber, and three-chamber views). The right ventricle (RV) can also be visualized using short axis LGE images, however, there may be scenarios where axial or HLA views are preferable, for example in arrhythmogenic right ventricular cardiomyopathy (ARVC) or congenital heart disease. Although the details of the LGE protocol may vary depending on the clinical indication, an appreciation for the fundamental principles of the technique will enable cardiovascular imagers to tailor this versatile technique to suit their specific clinical or research needs.

Contrast Kinetics

The first attempts to acquire T_1-weighted spin-echo images revealed that the T_1 of infarcted myocardium was distinctly prolonged compared to normal myocardium, resulting in regions of decreased signal intensity ('hypoenhanced' regions) [1, 4–7]. The introduction of paramagnetic contrast agents such as Gd-DTPA to cardiac MRI enabled stark delineation of irreversibly injured myocardium. Gadolinium (Gd3+) is paramagnetic and exerts an indirect T_1 (and to a lesser extent, T_2) shortening effect on neighboring water protons. The chelator, DTPA, is responsible for the distribution and kinetics of the contrast medium. Healthy cells with intact, selectively permeable cell membranes will exclude Gd-DTPA and therefore this agent is restricted to the extravascular and extracellular spaces (Fig. 15.1) [8, 9]. The loss of membrane integrity in irreversibly injured myocytes (e.g., in myocardial infarction) enables the contrast agent to enter the erstwhile intracellular space and, hence, increase its volume of distribution. Excess accumulation of Gd-DTPA is further exacerbated if there is ongoing ischemia and delayed washout kinetics, due to poor venous drainage [10].

One early approach toward quantifying the accumulation of Gd-DTPA in the myocardium was to immediately follow the bolus-injection by a constant-infusion of the contrast agent [11]. With this technique, equilibrium concentrations of the tracer can be achieved in the tissue, thus making it possible to estimate the partition coefficient (λ) of Gd-DTPA in ml of contrast medium per gram of myocardium [11]. Assuming normal renal clearance, an optimum constant infusion dose can be chosen such that the concentration of contrast agent will reach equilibrium in approximately 15 min, in all but the most severely ischemic regions of myocardium (perfusion <0.05 ml/min/g) [12]. With breakdown of cell membrane integrity, Gd-DTPA can begin to permeate the formerly intracellular space (Fig. 15.1c). Given that sarcolemmal disruption is a defining characteristic of irreversible injury, it follows that the λ in infarcted myocardium would exceed that of normal tissue and, in fact, it has been shown to be more than double that of normal myocardium (0.8 ml/g versus 0.3 ml/g) [11, 13, 14]. This has been validated in the setting of unreperfused infarction by Pereira and colleagues by a significant increase in λ in infarcted tissue as early as 2 days and for at least 3 weeks following permanent LAD occlusion in canine models [15]. When applied to patients with acutely reperfused AMI, λ was found to be inversely correlated to areas of low count-density on resting Tl-201 images [16]. Flacke et al. also demonstrated that λ can differentiate between normal and infarcted myocardium in patients with either acute or chronic myocardial infarction [17]. Considered together, the available evidence supports the conclusion that λ is increased exclusively in irreversibly injured myocardium.

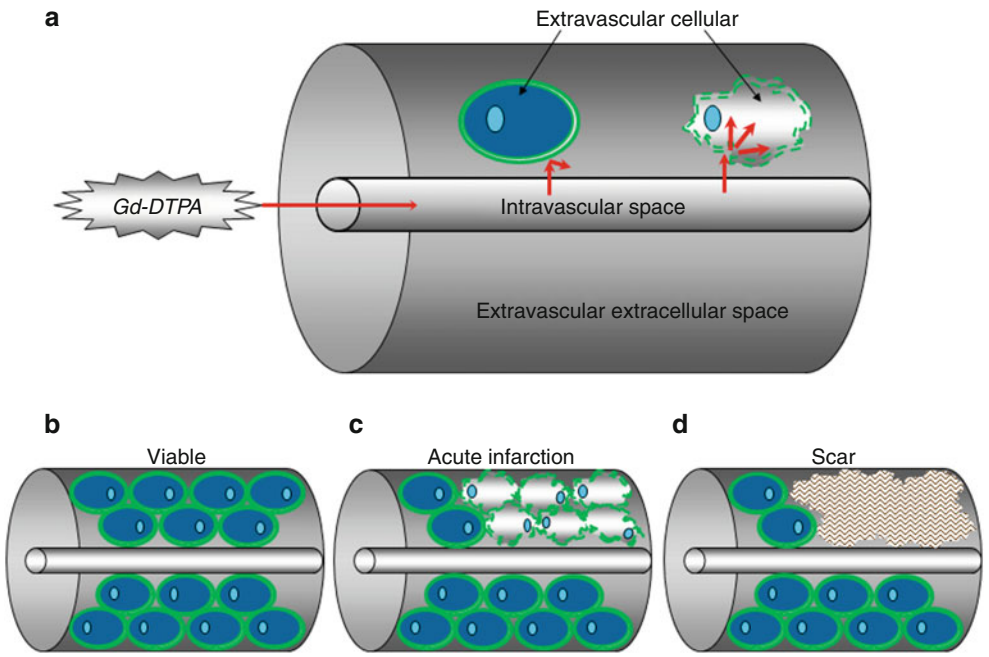

Fig. 15.1 A schematic depicting the distribution of Gd-DTPA contrast in myocardium (**a**), with two stylized cells, situated within a section of myocardium: a normal cell (*left*), with an intact, selectively permeable cell membrane, and an irreversibly damaged cell (*right*), with disrupted cell membranes. If we introduce an extravascular/extracellular contrast agent such as Gd-DTPA into the intravascular space, Gd-DTPA will not be able to penetrate the cell membrane of healthy myocytes, and therefore only distributes to the extracellular space (**b**). In acutely infarcted tissue, however, breaches in the cell membrane will permit the agent to enter the spaces previously occupied by the cell (**c**). In chronically infarcted or scarred myocardium (**d**), the remodelling process also results in a net decrease in the extravascular/cellular compartment, as the lost myocytes are ultimately replaced by mature, collagenous scar, into which Gd-DTPA can accumulate

With respect to dose, the convention at most institutions is to administer a "double dose," or 0.2 mmol/kg body-weight for all LGE exams. This is to ensure that maximum CNR between healthy and damaged myocardium is achievable at 10–20 min post-injection. Single dose imaging (i.e., 0.1 mmol/kg) will reduce the delay required between injection and image acquisition [18–21]. However, biological clearance of contrast occurs in a non-linear (exponential) fashion and therefore it is still preferable to wait at least 10 min post-injection prior to acquisition, regardless of dose so that areas of hyperenhanced myocardium will appear distinct from the LV or RV blood pools.

Nulling Normal Myocardium

The goal of LGE imaging is to null the signal contribution of healthy myocardium such that areas of scar or fibrosis are rendered as conspicuous as possible. We accomplish this by exploiting the difference in T_1 between healthy and fibrotic tissues. As such, all LGE sequences are T_1 weighted and most begin by means of a volume inversion preparation pulse. After the inversion pulse, the signal from healthy myocardium will recover according to a longer T_1 time than fibrotic myocardium. During this process, the magnetization from both healthy and fibrotic myocardium will pass through a point on the recovery curve where their contribution to the MR signal will be zero or "nulled." Identifying this inversion time (TI) or "null point" precisely for healthy myocardium is crucial for optimization of LGE imaging (Fig. 15.2). When the prescribed TI is too short, the longitudinal magnetization corresponding to normal myocardium will have a negative value during data readout and could potentially appear hyperenhanced relative to infarcted or fibrotic myocardium. Conversely, if the nominal TI is too long, the magnetization associated with normal myocardium will correspond to a point above the zero-crossing and appear gray, but not black (nulled) [22]. While irreversibly injured myocardium will appear hyperenhanced at long TIs, the CNR will be poor, since the discrepancy between the two tissues will be reduced.

There are essentially two different strategies for optimizing the TI: one can perform "test" LGE imaging using an initial "best guess" and then re-acquire in the appropriate direction to iteratively select the optimal inversion time. In practice, it is seldom necessary to perform more than two or three "re-tests" as an experienced technologist will be able to estimate the optimal TI merely from experience and a priori knowledge of the dose of contrast administered. For example, if we assume that normal myocardium has a post-contrast T_1 of 400 ms, then a patient with an R wave to R wave interval (R-R inter-

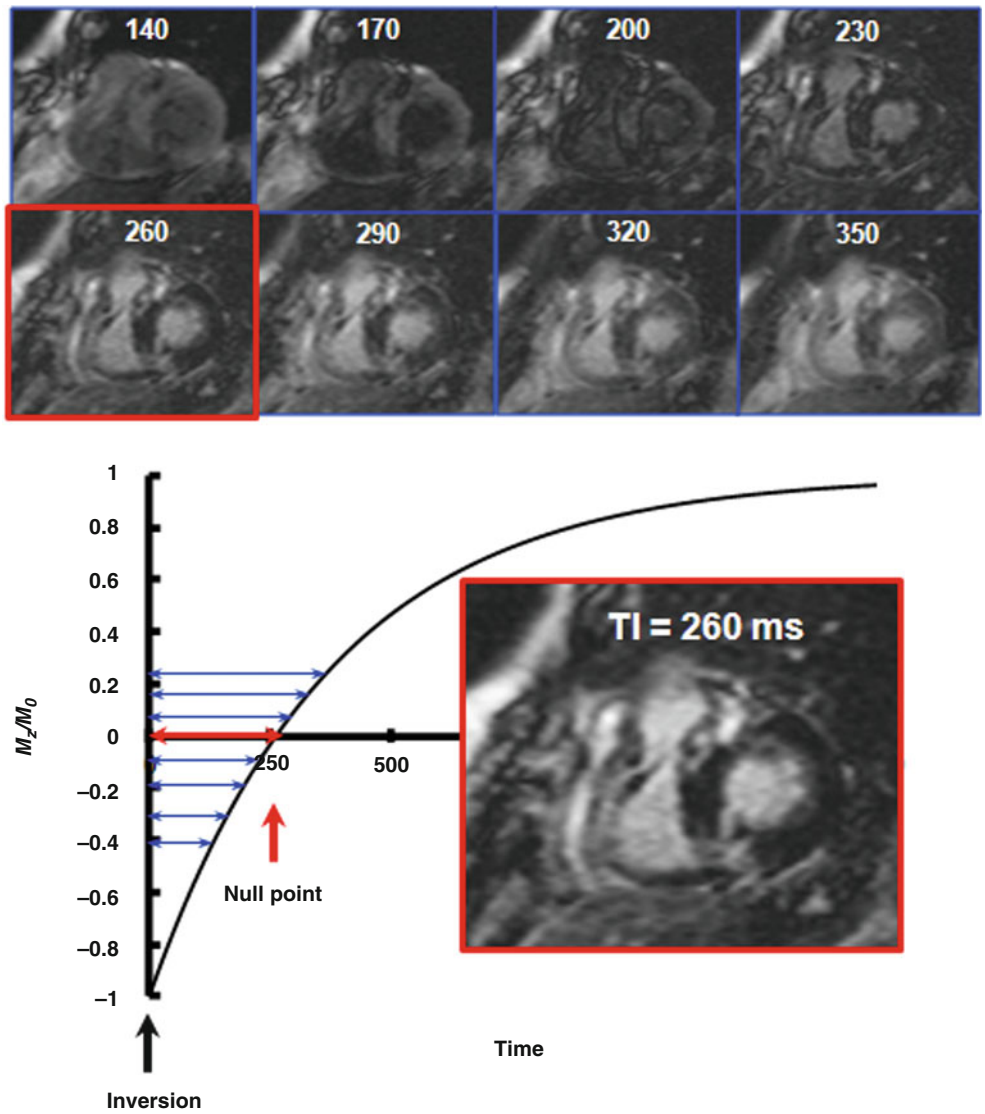

Fig. 15.2 Application of a "TI scout" sequence to determine the optimal TI for nulling normal myocardium. Eight short-axis scout images are shown (*top*) to illustrate the effect of TI on myocardial enhancement signal intensities in a patient with hypertrophic cardiomyopathy (the TI is indicated on the *top* of each image in ms). After a 180° inversion pulse at Time = 0, a series of images with incrementally increasing TIs are acquired during longitudinal relaxation (Mz/Mo). Note the increasing intensity of the fibrotic regions (at the RV-LV hinge points) with increasing TI. The time at which the longitudinal magnetization associated with normal myocardium passes through the Mz/Mo = 0 (null) point is recorded as the optimal TI. In this example, the optimal TI is determined to be 260 ms

val) = 800 ms will require an optimal inversion time of TI = ln (2)*T_1 = 0.69*T_1 = 280 ms [22]. Alternatively, most vendors provide a so-called "TI scout," which is usually an inversion recovery prepared cine sequence that systematically acquires test LGE images over a range of TIs (Fig. 15.2), enabling the operator to review and select the optimum inversion time prior to acquisition [23]. When using these sequences, it is important to remain cognizant of the fact that most TI scout sequences utilize a steady-state free precession readout, rather than the spoiled gradient-echo readout common to most LGE acquisitions. In practice, the optimal TI identified by the scout may not effectively match the true ideal required by the LGE sequence.

The Evolution of LGE Pulse Sequence Design

As previously discussed, the basic "recipe" for LGE imaging was first established in the 1980s. The penetration of the technique into mainstream imaging protocols in the last 10–15 years is primarily due to the near-continuous improvement and innovation in both MR hardware (gradient performance, RF coil sensitivity) and pulse sequence design. These advancements have culminated in the sequences we see on our scanners today: sequences that provide sufficient CNR and spatial resolution to resolve not only subendocardial infarcts, but post-ablation scars in the left atrium—achievements that would have been imponderable in the early days of ungated spin-echo LGE.

The preponderance of initial LGE studies published in the 1980s consisted of inversion-prepared spin-echo and fast ("turbo") spin-echo sequences [1, 2, 4, 5]. Although these sequences provided the T_1-weighting needed for delineating areas of gadolinium accumulation, the acquisition times were very long and made breath-holding impractical or impossible. Thus, respiratory artifacts degraded even the most rigorously acquired images. By the mid-to-late 1990s,

most of these spin-echo sequences had been replaced by faster gradient-echo varieties. Saturation- [13, 14, 24, 25] or inversion- preparation [26] provided the T_1-weighting, along with short TRs and shallow flip-angle readouts. Magnetization-driven "FLASH" (fast low-angle shot) techniques that involved constant RF pulsing also came on the scene at this time [27]. These gradient-echo techniques offered several advantages, as they were sufficiently rapid to be acquired within a reasonable breath-hold, and they could be comfortably repeated, to follow the temporal evolution of contrast accumulation. In fact, the single-shot saturation-prepared fast gradient-echo sequence was used for both perfusion and LGE imaging, and could be acquired either with or without a breath-hold, depending on the post-processing anticipated for quantitative analysis.

Segmented Inversion-Recovery Spoiled Gradient Echo

Unlike perfusion imaging, where the goal is to capture the rapid transit of contrast media during its first pass through the circulation, LGE imaging is performed 10–20 min after administration, to allow for the accumulation of Gd in the extravascular/extracellular space. At this stage, we assume that the contrast has reached equilibrium concentrations in the blood and the tissue. The T_1s are no longer changing very drastically and thus, it is no longer crucial to read out each image with high temporal resolution. Given that the goal is to obtain the optimum CNR between healthy and injured or fibrotic myocardium, most LGE imaging is now performed with segmented readout pulse sequences, such as the inversion-prepared spoiled gradient-echo sequence introduced by Simonetti et al. in 2001 [28]. This sequence represented a remarkable breakthrough in CNR, with infarct signal intensities 500–600 % greater than normal myocardium [21, 28, 29] (approximately tenfold improvement in CNR relative to T_1-weighted spin-echo sequences, for example). In this sequence, the initial inversion is achieved using a nonselective 180° pulse, which is typically a hyperbolic secant adiabatic inversion. Slice-selective inversion sequences have also been developed, and may improve edge-detection between healthy myocardium and scar. This could be particularly advantageous for imaging small areas of fibrosis or non-transmural infarcts [30].

A pulse sequence diagram for a typical implementation of the segmented inversion recovery spoiled gradient echo LGE sequence is depicted in Fig. 15.3. Before applying the initial inversion pulse, most scanners allow the technologist to select a variable delay time so that the image readout occurs at mid-diastole, or when we presume the heart is moving the least. We can then begin reading out the first segment of k-space after the pre-determined TI delay. Shallow flip-angle RF pulses (approximately 20–25°) are used during the readout of each line, so that the recovery of the post-inversion magnetization is largely unaffected and in accordance with the nominal TI. The size of the k-space segment (i.e., the number of lines of k-space) that we can read during each R-R interval will necessarily depend on the duration of diastole. In a typical implementation of the sequence [28], with a TR of 8 ms, a segment consisting of 23 lines of k-space can be acquired in 184 ms, which is within the period of mid-diastole for most patients. It is important to be cognizant that the segmented LGE sequences are more sensitive to arrhythmias and variable heart rates than their single-shot counterparts. While gradient-moment refocusing mitigates motion artefact to some extent, the duration of the mid-diastolic phase will also shorten with increasing heart rates, so the number of k-space lines acquired per R-R interval will have to be reduced to further minimize motion artifacts. The heart rate will also dictate sequence planning in terms of selecting the optimal inversion time. Unless the patient's heart rate is very slow (e.g., <50 bpm), the sequence is triggered every other heartbeat to allow sufficient longitudinal relaxation to occur between inversion pulses. The bulk magnetization M(t) will recover post-inversion according to the following: $M(t) = M_o(1 - 2e^{-t/T_1})$. Thus, if we return to our earlier example with the patient (R-R interval = 800 ms), normal myocardium with a post-contrast $T_1 = 400$ ms will require approximately $4 \times T_1 = 1{,}600$ ms to recover approximately 96 % of its bulk magnetization.

Phase-Sensitive Inversion-Recovery Imaging

The advent of phase-sensitive reconstruction LGE sequences in 2002 [31] has greatly improved the consistency of image quality over a wide range of TIs, particularly with respect to the CNR between infarcted and normal myocardium [32]. Recall from our earlier discussion that the longitudinal magnetization associated with infarcted or fibrotic myocardium will recover more quickly than that of normal myocardium, since its T_1 is shorter. With conventional magnitude reconstruction, if we prescribe a TI that is too short to null normal myocardium, then the normal myocardium will appear too bright and the CNR between normal and infarcted or fibrotic myocardium will be poor. Even when care is taken to isolate the optimal TI for the first slice (e.g., the first of a short-axis stack covering the LV), the continued clearance of contrast over the 5 min multi-slice acquisition will mean that the T_1 will have increased non-negligibly by the time the final slice is acquired. Phase-sensitive detection is insensitive to small drifts in T_1, enabling the acquisition of a full complement of high CNR images without the need to interrupt the acquisition to repeat the search for optimal TI. The phase-sensitive detection aspect of this technique involves the acquisition of reference phase maps in between the collection of inversion recovery data (Fig. 15.3, gray inset). These phase images

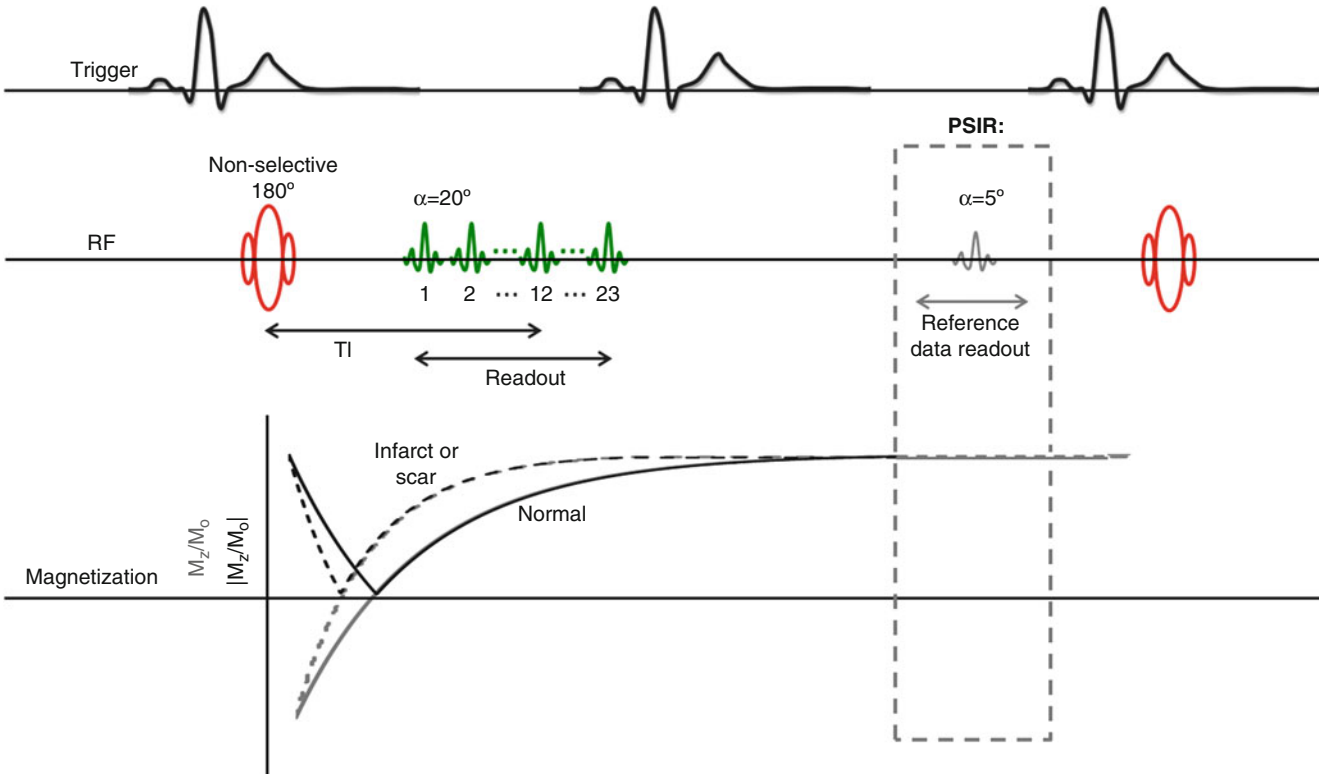

Fig. 15.3 Pulse sequence diagram and associated longitudinal magnetization for a segmented inversion-recovery spoiled gradient echo sequence. The phase-sensitive modification for this sequence is indicated in gray. In both sequences, the non-selective inversion pulse is triggered following a variable delay following detection of the R-wave so that readout occurs at mid-diastole. The first segment of k-space is acquired after the inversion delay TI using shallow flip angle pulses (20°). In this example, each segment consists of 23 lines of k-space. The subsequent segment is collected after allowing for sufficient recovery of longitudinal magnetization, which for most cases translates to every other heartbeat. In the phase-sensitive modification of this sequence (*gray*), these quiet periods between inversion pulses are used to collect reference images using very shallow RF pulses (5°), so that longitudinal recovery is not unduly disrupted. These reference images are used to remove the background phase from the IR images during reconstruction and restore the signal polarity of the image. For phase-sensitive images, the image intensity is displayed as Mz/Mo (*gray recovery curves*) rather than the |Mz/Mo| seen in magnitude reconstructed images (*black recovery curves*)

include information regarding background phase as well as surface coil field maps. The phase can be subsequently removed from the IR image during reconstruction to reveal the real component of the inversion recovery image. By restoring the signal polarity of the image, phase-sensitive reconstruction effectively avoids the enhancement artifacts to which magnitude images are prone.

3D and Free-Breathing Techniques

All of the LGE sequences discussed thus far involve 2D imaging, or the acquisition of one 2D slice per breath-hold. Depending on the indication for LGE imaging, comprehensive coverage could potentially involve more than ten breath-holds, which can prove difficult for some patients, particularly those with advanced disease. Fortunately, many scanners are also equipped with 3D LGE sequences, in which the entire LV can be imaged in a single (albeit long) breath-hold. In most implementations, 3D LGE is accomplished using a segmented inversion-recovery gradient echo sequence with shallow flip-angle readout (e.g., 15° rather than the 25° typical of most 2D acquisitions). In 3D LGE, the inversion pulse is triggered every heartbeat (instead of every second heartbeat), which can potentially degrade CNR due to incomplete magnetization recovery. Approximately 20 contiguous sections are acquired in the z direction, often with the aid of zero-filling and interpolation to maximize spatial resolution in this direction [33]. If the breath-hold required to cover the LV is potentially too long, the LV can be covered in a quasi-3D fashion by dividing the acquisition into three "slabs," with a commensurate number of manageable breath-holds [34]. While the strategy for finding the optimal TI should be the same as described for 2D LGE, the advantage is that this TI need only be selected once. The correct TI is particularly crucial for 3D imaging, as there is no opportunity to utilize alternate R-R intervals for acquiring reference images for phase-sensitive reconstruction. Additionally, the need to trigger every heartbeat results in greater sensitivity to arrhythmias. Optimization of 3D acquisitions is a subject of considerable ongoing research. While breath-hold 3D slab acquisitions are promising, they may still present difficulties

for some patients. In 2004, Saranathan and colleagues presented a free-breathing 3D LGE alternative, in which a navigator-echo segment is acquired immediately following the gradient echo acquisition [35]. The navigator echo segment is essentially a spin echo sequence that selects a column of spins craniocaudally across the right hemidiaphragm [36]. When combined with their hybrid k-space segmentation scheme, the free-breathing sequence proposed by Saranathan et al. was capable of acquiring 16×5 mm thick sections in less than 2 min.

Common Clinical Applications

LGE has become an undeniably powerful tool for the assessment of many clinical cardiac entities. While much of the early development of LGE imaging was centered on the assessment of post-infarction scar, the technique has become increasingly valuable in the characterization of a wide variety of cardiomyopathies as well as in the rule-out of infectious or infiltrative disease. This section is far from an exhaustive accounting of the myriad applications of LGE imaging. Rather, the intention of the following discussion is to illustrate how the technique has been adapted to address a variety of clinical and research questions.

Acute and Chronic Myocardial Infarction

In many ways, the assessment of myocardial viability and infarct scar was the driving force behind the initial development of LGE imaging. Before the advent of the high CNR segmented inversion-recovery gradient echo techniques, most studies were limited to pre-clinical research in rats [37–42] and dogs [43–47] and small "proof of principle" clinical series [16, 17, 19, 21, 26, 29, 48–52]. The veritable explosion of reports involving LGE imaging in the last decade belies the fact that we owe a great deal of its current appeal to the fundamental basic science and development that preceded this recent popularity.

Many of the early contributions to the development of the technique were focused on establishing the kinetics of MR contrast in ischemic and infarcted myocardium. Specifically, there was a great deal of debate regarding the distribution of Gd-DTPA in areas of reversibly injured myocardium [41, 53]. In a rat model of reperfused infarction, Saeed and colleagues found that Gd-DTPA enhanced regions were 33 % larger than the extent of infarcts identified by triphenyltetrazolium chloride (TTC) staining at day 2 post-reperfusion [40], suggesting that reversibly injured myocardium might also accumulate Gd-DTPA. However, similar studies in canine models such as the one reported by Fieno and colleagues, found excellent agreement between both *in vivo* and *ex vivo* gadolinium enhanced images and TTC staining (r = 0.95) [47], which supports the notion that myocardial hyperenhancement is specific to irreversible injury (infarction). Establishing the "bright equals dead" principle was a key step, as the management of patients with coronary artery disease (CAD) post-infarction is complicated by the presence of both reversibly damaged and infarcted myocardium. The success of revascularization depends on both the existence and extent of viable but dysfunctional myocardium present, as there are few benefits from revascularizing a territory devoid of viable myocardium. Infarction follows a characteristic path or "wavefront" in the myocardium, beginning in subendocardial tissue and progressing towards the subepicardium. Nuclear medicine methods that are often used for assessing myocardial perfusion (e.g., PET, Tl-201, Tc-99m-sestamibi SPECT) lack the ability to resolve transmural variations in viability. LGE CMR, however can identify subendocardial infarcts that would be otherwise missed by Tc-99m-sestamibi SPECT, for example [20]. Choi et al. investigated the relationship between the transmural extent of LGE hyperenhancement and long-term functional improvement in AMI patients at 1 week and 8–12 weeks following reperfused-infarction [18]. In this important work, the authors showed that the extent of the dysfunctional but normally enhancing region at 1 week post-reperfusion was the single best predictor of functional recovery 8–12 weeks post-reperfusion.

In acutely infarcted myocardium, cell membranes lose their integrity and the Gd-DTPA suddenly gains access to what was formerly intracellular space and shortens T_1 to a much greater extent than if the agent was in contact with extracellular space alone. In contradistinction, there does not appear to be an increase in the distribution volume of Gd-DTPA in reversibly dysfunctional myocardium (i.e., "stunned" or "hibernating" myocardium). The ultrastructural changes typical of hibernating myocardial cells include a progressive loss of contractile proteins, which are predominantly replaced by glycogen within the cytoplasm. However, there is no appreciable decrease in cell volume and therefore no evidence of increased gadolinium distribution in hibernating myocardium [51, 54]. Similarly, there does not appear to be any hyperenhancement associated with transiently dysfunctional or "stunned" myocardium [55, 56], which has been confirmed by high-resolution Gd-enhanced imaging of ex-vivo specimens.

Although we conceptualize LGE imaging as "viability" or "scar" imaging, there are certainly settings where perfusion has an outsized influence on late enhancement patterns. One such scenario is in unreperfused infarction, where microvascular damage can severely impede contrast wash-in to the myocardium. On LGE images, microvascular obstruction can manifest as a persistent core of hypoenhancement surrounded by hyperenhancement. Interestingly, this core appears to

involute as the infarct heals, regardless of reperfusion status. As the initial inflammation begins to subside and macrophages have left with their cargo of necrotic debris, type I collagen is deposited into the infarcted region. By this point, there should be no residual capillary plugging interfering with Gd-DTPA distribution [57]. Infarct remodelling involves organization of the collagenous scar, with a concomitant loss of myocytes. The net result is a predominantly acellular area, and one that an extravascular/extracellular agent such as Gd-DTPA can occupy in observable volumes (Fig. 15.1d) [58]. Additionally, the potential recruitment of collateral circulation should not be neglected, as it may partially contribute to Gd-DTPA distribution as the infarct matures. Wu et al. demonstrated that LGE hyperenhancement was present in both Q wave and non-Q wave infarcts at 3 months and 14 months following acute myocardial infarction (AMI), and yet none of the patients in the comparison group with idiopathic dilated cardiomyopathy (DCM) exhibited hyperenhancement [21]. This was consistent with the findings reported by Klein et al. in a group of patients with chronic CAD and severely reduced LV function. Klein and colleagues demonstrated that LGE can delineate the location and extent of nonviable myocardium, in close agreement with NH_3/FDG PET measurements of perfusion and glucose metabolism [51]. In fact, the authors demonstrated that the sensitivity and specificity of hyperenhancement for detecting either transmural or non-transmural scar tissue (as defined by NH_3/FDG PET mismatch) were 83 % and 88 %, respectively.

Ischemic Cardiomyopathy

The term ischemic cardiomyopathy is often used by clinicians to describe chronic ischemic heart disease, such as that experienced by patients with post-infarction remodelling and LV dysfunction. As with post-infarct LGE, the hyperenhancement associated with "ischemic type" cardiomyopathy has three main characteristics: it always involves the subendocardial layer, it is localized in the territories supplied by the epicardial coronary arteries, and it is consistent with regional wall motion abnormalities (Fig. 15.4). Furthermore, ischemic cardiomyopathy is inconsistent with hyperenhancement located exclusively in the subepicardium or mid-myocardium [59].

When a patient initially presents with LV dysfunction, one of the first objectives is to determine whether the dysfunction arises from an ischemic etiology and if so, the next most important objective is to assess if the myocardium is viable. In a meta-analysis, Allman et al. showed that revascularization may reduce annual mortality in up to 80 % of patients with LV dysfunction and viable myocardium when compared to medical treatment [60]. Kim et al. [29] showed that segments demonstrating ≤50 % of transmural extent of hyperenhancement are likely to recover function after revascularization.

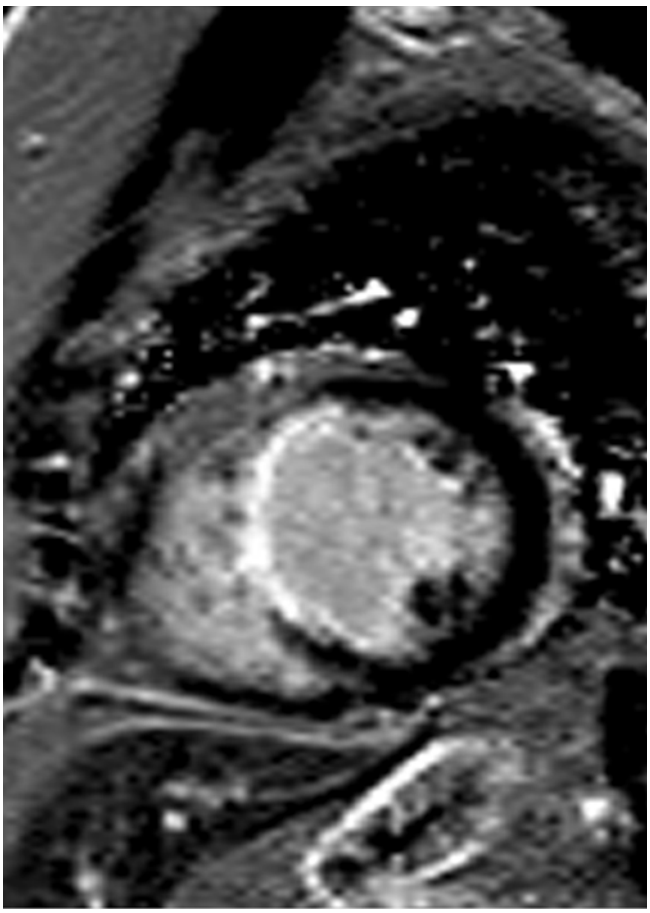

Fig. 15.4 70-year-old woman who presented with dilated cardiomyopathy and an ejection fraction of 35 %. Coronary angiography demonstrated 100 % stenosis in the mid left anterior descending coronary artery. Cardiac MR was performed to assess myocardial viability. Late gadolinium enhancement phase sensitive inversion recovery image in short axis view demonstrates transmural extent of enhancement in the mid septal wall in a left anterior descending artery territory diagnostic of a prior myocardial infarction

Non-ischemic Cardiomyopathies

To increase the likelihood of clinical improvement in patients with cardiomyopathy, proper determination of the etiology is essential as it then guides proper management. While the cause of non-ischemic cardiomyopathies (NICM) can theoretically be confirmed via endomyocardial biopsy, in practice this invasive approach offers limited sensitivity, particularly for conditions in which myocardial fibrosis or infiltrate may be sparse or heterogeneous in distribution [61]. LGE CMR is not only a key tool for differentiating between ischemic and NICM, it is also crucial for differential diagnosis, since several cardiomyopathies have been associated with their own "signature" enhancement patterns. Ultimately, these patterns that are summarized in the following section may also be used to guide endomyocardial biopsy, helping secure a histopathological diagnosis.

Dilated Cardiomyopathy

After a thorough medical history, including family history, and examination with laboratory testing have been conducted, CMR is often considered as an essential part of the diagnostic evaluation for patients with DCM of unknown cause. While echocardiography and CMR both demonstrate ventricular enlargement and decreased systolic function as measured by ejection fraction, McCrohon et al. [62] showed that the midwall enhancement pattern by LGE-CMR typified non-ischemic DCM. Figure 15.5 demonstrates an example of a patient with new onset heart failure and this characteristic enhancement pattern. Of note, 13 % of DCM patients in this cohort previously labeled as nonischemic DCM based on nonobstructive coronary arteries at by invasive angiography actually had subendocardial infarct scar. This suggested a prior myocardial infarction with recanalization or dispersion of an embolic source, with cardiac enlargement and systolic function ensuing as a result of post-infarct adverse remodeling. Midwall enhancement has been identified as an adverse prognostic finding, predicting events such as sudden cardiac death and heart failure with incremental value beyond ejection fraction [63].

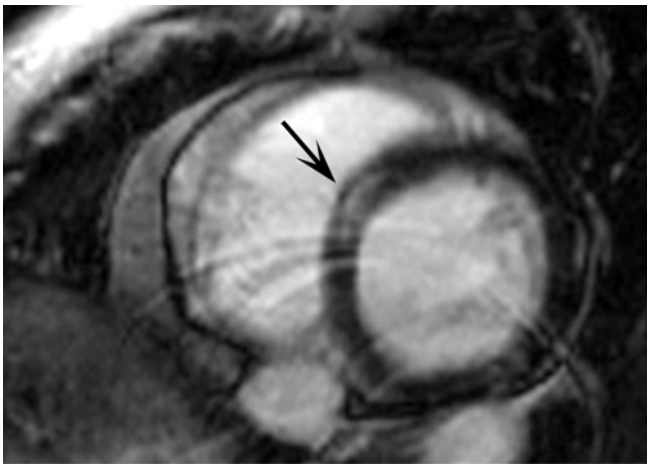

Fig. 15.5 Dilated cardiomyopathy in a 54-year-old man who presented with heart failure. Late gadolinium enhancement magnitude inversion recovery image in a short axis plane demonstrates a characteristic linear mid-myocardial hyperenhancement in the basal septum (*arrow*)

Hypertrophic Cardiomyopathy

HCM, typically due to mutations in genes encoding for sarcomeric proteins, is characterized by a cardiac phenotype with myocardial disarray, hypertrophy and fibrosis. Early diagnosis of HCM is crucial, as it remains both the most common cause of SCD among young people [64] and a not infrequent cause of heart failure. Given the varied clinical and phenotypic manifestations of the disease, HCM can pose a considerable diagnostic challenge [65]. Non-invasive markers for focal myocardial fibrosis can potentially track progression to heart failure in patients with HCM and help characterize the risk of SCD. Positive LGE occurs in up to 80 % of patients with HCM [66–68] and represents replacement myocardial fibrosis histologically [29, 69]. The typical LGE pattern in HCM is patchy and in a non-coronary distribution, most commonly associated to the regions of hypertrophy such as the insertion points of the interventricular septum in the classic asymmetric septal hypertrophy phenotype [67, 70–72]. Its presence is an independent predictor of adverse outcomes in HCM [72–76]. An example of the pattern of scarring typically observed in HCM is provided in Fig. 15.6.

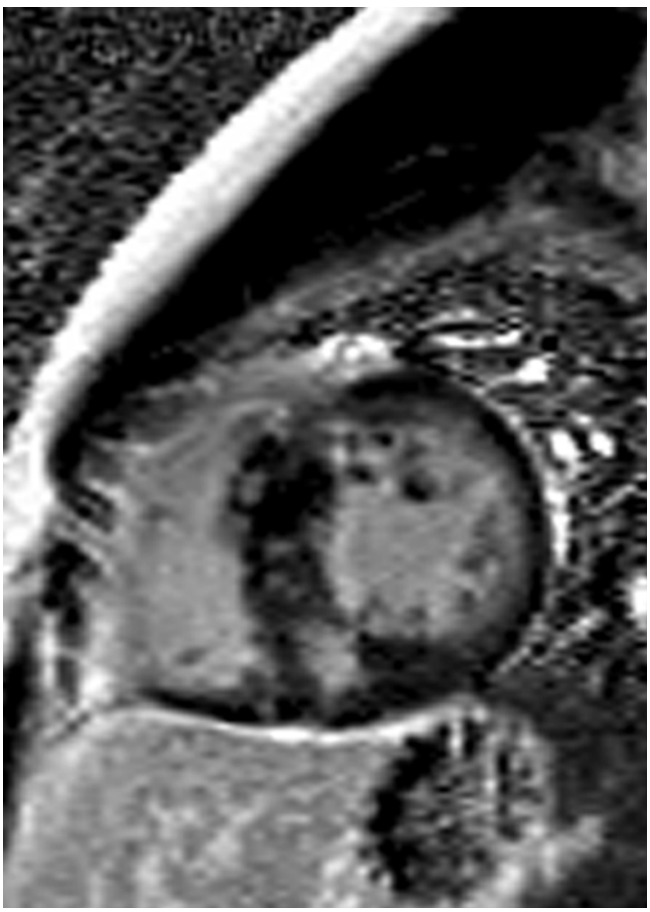

Fig. 15.6 Hypertrophic cardiomyopathy in a 18-year-old man presenting with multiple syncopal episodes. Late gadolinium enhancement phase sensitive inversion recovery image in a short axis plane demonstrates patchy, mid-myocardial enhancement matching the regions of hypertrophy in the septum

Arrhythmogenic Right Ventricular Cardiomyopathy

ARVC is a progressive cardiomyopathy due to fibrofatty replacement of normal myocytes that is associated with right heart failure and SCD. Like HCM, accurate diagnosis of ARVC is important for the prevention of SCD [77, 78]. ARVC is particularly difficult to diagnose, as several of the

presentations of ARVC can mimic that of cardiac sarcoidosis (CS). Furthermore, biopsy for the diagnosis of CS or ARVC is frequently inaccessible owing to the random and patchy distribution of fibrofatty infiltration along the RV septum. It is important to mention that abnormal LGE is not included in the new Task Force Criteria for the diagnosis of ARVC [79], which are based on the presence of increased RV size, decreased RV EF, and RV wall motion abnormalities. Nevertheless, Steckman and colleagues recently reported that LGE hyperenhancement was seen in 73 % of CS and 19 % of ARVC patients, with isolated LV involvement seen only in the CS group [80]. Forty-three percent of the CS group and none of the ARVC group demonstrated intraventricular septum dysfunction or hyperenhancement of the septum. Septal enhancement was observed in 78 % of those with CS and 0 % of those with ARVC. Given the overlap in clinical presentation and high false-negative rate of endomyocardial biopsy, a tool for the accurate differentiation of these conditions is needed.

Cardiac Sarcoidosis

Sarcoidosis is a granulomatous disease affecting multiple systems. It is estimated that 5 % of patients with pulmonary/systemic sarcoidosis also have symptomatic CS [81], which is belied by the higher prevalence observed in necropsy studies [82, 83]. Missing the diagnosis of CS can lead to increased mortality due to SCD or heart failure. LGE MRI findings have been documented in both acute and chronic stages, but enhancement patterns can vary widely [84–87]. While hyperenhancement in CS is often localized to the epicardial zone of the septum, the fibrosis can appear either focal, patchy, or even extend to fully transmural hyperenhancement [87], as observed in the example provided in Fig. 15.7. Also LGE characteristically involves the basal anteroseptal and anterolateral segments of the LV [84]. Early evaluations of LGE in the setting of CS suggested that its sensitivity was significantly inferior to PET [88]. More recent analyses demonstrate that LGE may detect CS at a twofold higher rate than conventional Japanese Ministry of Health criteria (12-lead ECG and either echo, radionuclide perfusion, or cath imaging) [87]. Patel and colleagues [87] found that LGE detected CS in 26 % of patients with biopsy-proven extracardiac sarcoidosis, compared to 12.3 % identified using Japanese Ministry of Health criteria. Furthermore, the authors showed that positive LGE findings were the only independent predictor of adverse clinical events.

Myocarditis

The clinical presentation of myocarditis may mimic acute myocardial infarction in patients with normal coronary arteries on angiogram [89]. Although endomyocardial biopsy is the standard of reference for the differentiation between these two entities, LGE plays an important role in non-invasively distinguishing both entities [90]. Friedrich and colleagues were among the first to report myocardial enhancement patterns in patients with acute myocarditis [91]. Using a non-breath-hold T_1-weighted spin-echo pulse sequence, the authors demonstrated 40–50 % greater hyperenhancement in patients with myocarditis, suggesting that LGE even with the low CNR pulse-sequence could identify areas of inflammation. This discrepancy in enhancement was exaggerated to 400 % above normal myocardium when the segmented IR-prepared fast GRE approach was applied to 32 patients with suspected myocarditis [90].

In addition to colocalizing regions of hyperenhancement with histopathologically-confirmed areas of active myocarditis, Marholdt and colleagues observed a distinct geographic pattern from ischemic LGE enhancement, affecting the epicardial quartile of the LV or midwall region [90]. An example of this characteristic enhancement

Fig. 15.7 48-year-old woman presenting with heart block. Late gadolinium enhancement phase sensitive inversion recovery image in a short axis view demonstrates transmural enhancement in the basal septal and anteroseptal walls (*arrow*) characteristic of cardiac sarcoidosis

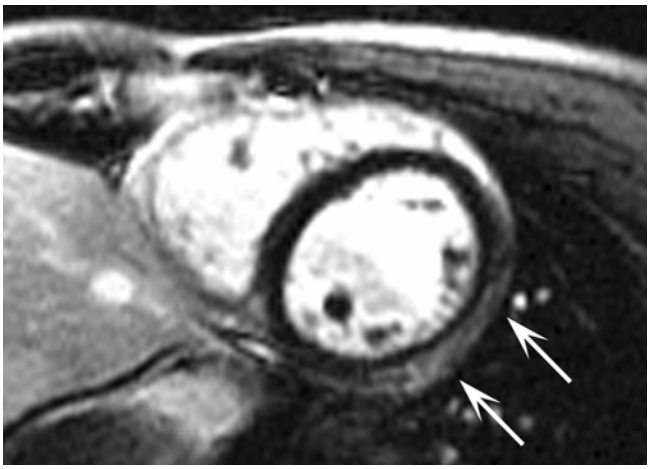

Fig. 15.8 Myocarditis in a 16-year-old male who presented with chest pain and ST elevation on the ECG. Late gadolinium enhancement magnitude inversion recovery image in a short axis view demonstrates subepicardial enhancement in the mid lateral wall (*arrows*) indicative of myocarditis. Note that the subendocardium is nulled, excluding an ischemic cause

pattern is provided in Fig. 15.8. They suggested that the mechanism for LGE during the acute phase of myocarditis is myocardial necrosis, whereas in the more chronic phase, LGE likely represents fibrosis [90]. The areas of LGE may decrease during recovery of myocarditis and can nearly resolve after recovery.

Amyloidosis

Cardiac amyloidosis (CA) is characterized by the interstitial deposition of insoluble amyloid proteins. It presents as a restrictive cardiomyopathy and it is one of the differential diagnoses when assessing patients with diastolic heart failure and myocardial hypertrophy [92]. The gold standard for diagnosing CA is endomyocardial biopsy, but this technique is invasive and has associated risks [93]. A characteristic LGE "amyloid pattern" has been described as diffusely distributed over the entire subendocardial circumference, extending in various degrees into the neighboring myocardium and coupled with a dark black blood pool [94–96]. This distinct pattern of enhancement (Fig. 15.9) is present in approximately 80 % of patients with CA [94, 95, 97] and has shown a sensitivity of 80 % and specificity of 94 % for the diagnosis of CA compared to endomyocardial biopsy [95].

In practice, it can be difficult to establish the appropriate TI for nulling normal myocardium in patients with CA [94], even with the benefit of a TI scout. Maceira et al. reported that blood pool gadolinium clearance was faster than normal in CA patients and that the areas with amyloid deposition demonstrate T_1s either shorter than or equivalent to those sampled in the blood pool [94]. Additionally, the contrast between normal myocardium and areas of amyloid deposition becomes markedly reduced approximately 8 min after contrast administration. Thus, LGE images in patients with cardiac amyloidosis are ideally acquired between 5 and 8 min post-injection when the contrast between normal and abnormal myocardium, compared to the typical delay of 10–15 min [94]. Multiple theories have been proposed to explain the contrast kinetics idiosyncratic to CA, the foremost of which is that the marked expansion of the extracellular space is due to accumulation of the interstitial amyloid protein [94, 96, 97], rather than diffuse fibrosis, but this is an active area of investigation. Contemporary quantitative T_1 mapping techniques, covered elsewhere, have greatly reduced uncertainty in the interpretation of LGE images in cardiac amyloidosis.

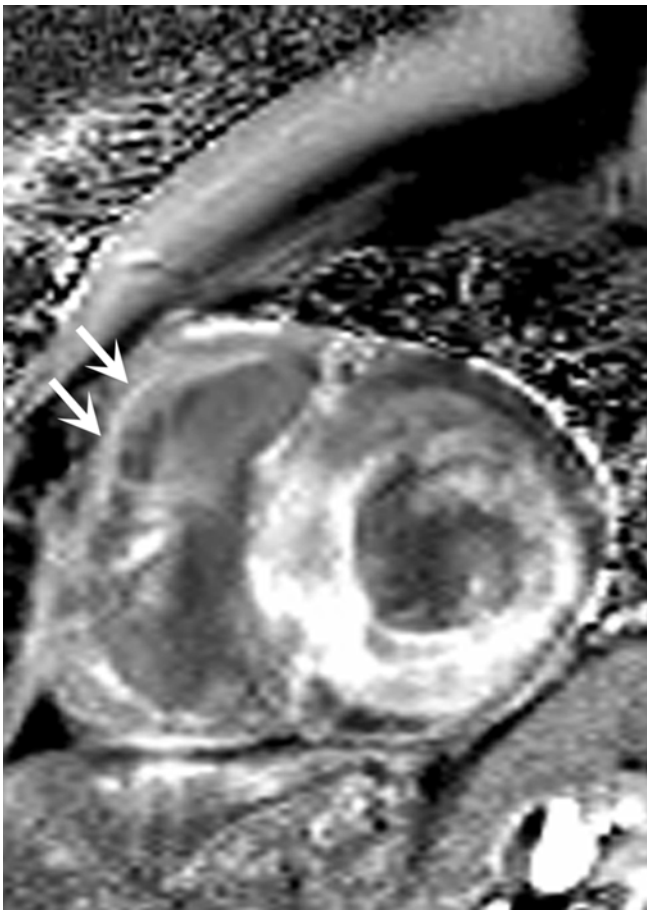

Fig. 15.9 75-year-old man presenting with unexplained severe left ventricular hypertrophy, chronic heart failure and atrial fibrillation. Cardiac MR was performed to exclude an infiltrative cardiomyopathy. Late gadolinium enhancement phase sensitive inversion recovery image in a short axis plane demonstrates diffuse subendocardial enhancement in the left ventricle with a variable extent to the adjacent myocardium. There is also subendocardial enhancement present in the right ventricle (*arrows*). Note that the blood pool shows a characteristic dark appearance commonly observed in cardiac amyloidosis

Other Indications

Cardiac and Pericardial Masses

Evaluation of a cardiac mass is a common indication for cardiac MRI. Although the use of LGE in the evaluation of cardiac masses is beyond the scope of this chapter, we will review its use in the assessment of thrombus since it is the most common cardiac mass. Thrombus is a differential diagnosis for cardiac tumors, and is typically identified in the LV as a result of dysfunction and impaired wall motion following myocardial infarction. LGE imaging can be a helpful technique for differentiating thrombi from masses, since thrombus is avascular and thus, will appear as a mass of low signal intensity on LGE images. It is not uncommon for thrombi to appear as hypoenhanced masses adjacent to areas of hyperenhanced myocardial infarction [98], as shown in Fig. 15.10. The use of LGE imaging with a long TI to null avascular tissue (600 ms) is a strategy to characterize thrombus [99].

Left Atrial Remodeling and Scar

Perhaps one of the most exciting developments in recent years has been application of LGE to the assessment of left atrial remodeling and scar. The left atrium (LA) has long been considered "uncharted territory" in CMR, given its thin walls and potential interference from neighboring fat. The advent of free-breathing 3D LGE schemes enabled researchers to begin exploring LGE as a tool for evaluating LA fibrosis. Peters et al. adapted the sequence proposed by Saranathan and colleagues [35] for evaluating post-ablation LA scar in patients with atrial fibrillation (AF) [100]. By combining the navigator-gated 3D LGE sequence with strategic fat saturation, the authors achieved a voxel size of 1.3×1.3×5 mm (reconstructed to 0.6×0.6×2.5 mm), sufficient to visualize focal hyperenhancement caused by pulmonary vein radiofrequency ablation. Oakes and colleagues evaluated a very similar sequence in patients with AF, but performed imaging prior to ablation in order to assess the potential of 3D LGE to predict procedural outcomes [101]. In addition to finding a significant positive correlation between areas of LA fibrosis on LGE and low-voltage regions on electroanatomic maps ($R^2=0.61$, $P<0.05$), the authors indicated that there was a strong association between pre-ablation hyperenhancement and post-procedural recurrence of AF. Specifically, patients who experienced post-procedural AF exhibited hyperenhancement throughout the LA. In contradistinction, the hyperenhancement observed among treatment responders appeared to be restricted to the posterior wall and septum. This important work suggests that 3D LGE shows potential to guide clinicians in predicting who will benefit from catheter ablation of AF.

Fig. 15.10 Anterior myocardial infarction in a 30-year-old man who presented with chest pain, troponin elevation, and echocardiographic abnormalities after receiving a hematopoietic stem cell transplant. Late gadolinium enhancement magnitude inversion recovery image in a four-chamber view demonstrates subendocardial enhancement in the left anterior descending coronary artery territory of distribution (*short arrows*). The mass in the left ventricle does not demonstrate enhancement, indicating an associated intraventricular thrombus (*long arrow*). The combination of a non-enhancing mass adjacent to an area of infarcted myocardium is highly suggestive of a thrombus

Image Interpretation and Quantification

As we have seen, LGE imaging has undergone tremendous technical evolution since its introduction in the early days of cardiac MRI. In view of this pedigree, it is somewhat surprising that there is no consensus about quantification of these images. Many radiologists and cardiologists continue to rely on subjective visual assessment or semi-quantitative techniques for routine interpretation of LGE images. Borrowing the 17 segment AHA model familiar to cardiologists, some clinicians report the extent of hyperenhancement in terms of the approximate area per AHA segment (e.g., 0–25 %, 25–50 %, etc.) [29]. If dedicated post-processing software is available, it is often possible for the analyst to select a reference area of "normal" (ideally nulled) myocardium, such

that all pixels in excess of a pre-defined number of standard deviations of that reference become defined as "hyperenhanced." Society for Cardiovascular Magnetic Resonance guidelines [102] recommend defining "hyperenhancement" as any myocardial pixel exceeding the mean signal intensity of normal myocardium by more than two standard deviations (SDs), but many programs allow flexible selection of between 2 and 6 SDs. Others have advocated for a "full width at half maximum" (FWHM) technique, in which the scar is selected by the analyst and the threshold for hyperenhancement becomes the value of the 50 % maximum signal intensity within the scar [103]. Flett et al. compared the LGE volumes obtained using seven distinct quantification techniques (manual segmentation, FWHM, or thresholds equal to 2, 3, 4, 5 or 6 SD above normal myocardium) in patients with AMI, chronic MI (CMI), and HCM [104]. The authors discovered that the LGE volumes defined by each of the methods varied substantially, and the most reproducible techniques appeared to depend on the clinical entity under investigation (e.g. AMI, CMI, or HCM). Specifically, the 2-SD threshold resulted in infarct volumes as high as 100 % greater than either the FWHM, 6-SD or manual approaches. The effect of threshold was most apparent in the HCM patients, where hyperenhanced volumes varied from 11 to 29 %. For both infarct-size estimates and HCM fibrosis quantification, the authors recommended either the 6-SD or FWHM thresholds. The limitation of the FWHM approach is that it assumes that maximum hyperenhancement will be localized to the lesion core, which can be problematic in the case of heterogeneous or "patchy" enhancement.

Conclusion

Over the last 30 years, LGE imaging has evolved from a relatively esoteric research interest to an indispensable component of most clinical CMR examinations. While the sequence and implementation may differ depending on availability and indication, a firm understanding of the principles underpinning LGE will assist in providing important diagnostic and prognostic information relevant for patient care.

References

1. Ratner AV, Okada RD, Newell JB, Pohos GM. The relationship between proton nuclear magnetic resonance relaxation parameters and myocardial perfusion with acute coronary arterial occlusion and reperfusion. Circulation. 1985;71(4):823–8.
2. Wesbey G, Higgins CB, Lanzer P, Botvinick E, Lipton MJ. Imaging and characterization of acute myocardial infarction in vivo by gated nuclear magnetic resonance. Circulation. 1984;69:125–30.
3. McNamara MT, Higgins CB, Ehman RL, Revel D, Sievers R, Brasch RC. Acute myocardial ischemia: magnetic resonance contrast enhancement with gadolinium-DTPA. Radiology. 1984;153:157–63.
4. Johnston DL, Brady TJ, Ratner AV, Rosen BR, Newell JB, Pohost GM, Okada RD. Assessment of myocardial ischemia with proton magnetic resonance: effects of a three hour coronary occlusion with and without reperfusion. Circulation. 1985;71(3):595–601.
5. Pflugfelder PW, Wisenberg G, Prato FS, Carroll SE, Turner KL. Early detection of canine myocardial infarction by magnetic resonance imaging in vivo. Circulation. 1985;71(3):587–94.
6. Bouchard A, Reeves RC, Cranney G, Bishop SP, Pohost GM. Assessment of myocardial infarct size by means of T_2-weighted 1H nuclear magnetic resonance imaging. Am Heart J. 1989;117:281–9.
7. Ryan T, Tarver RD, Duerk JL, Sawada SG, Hollenkamp NC. Distinguishing viable from infarcted myocardium after experimental ischemia and reperfusion by using nuclear magnetic resonance imaging. J Am Coll Cardiol. 1990;15:1355–64.
8. Wesbey G, Weinmann HJ, Brasch RC, Press WR. Characteristics of gadolinium-DTPA complex: a potential NMR contrast agent. AJR Am J Roentgenol. 1984;142:619–24.
9. Prato FS, Wisenberg G, Marshall TP, Uksik P, Zabel P. Comparison of the biodistribution of gadolinium-153 DTPA and technetium-99m DTPA in rats. J Nucl Med. 1988;29:1683–7.
10. Judd JR, Kim RJ, Chen EL, Lima JA. Myocardial Gd-DTPA kinetics determine MRI contrast enhancement and reflect the extent and severity of myocardial injury after acute reperfused infarction. Circulation. 1996;94(12):3318–26.
11. Diesbourg LD, Prato FS, Wisenberg G, Drost DJ, Marshall TP, Carroll SE, O'Neill B. Quantification of myocardial blood flow and extracellular volumes using a bolus injection of Gd-DTPA: kinetic modeling in canine ischemic disease. Magn Reson Med. 1992;23(2):239–53.
12. Tong CY, Prato FS, Wisenberg G, Lee TY, Carroll E, Sandler D, Wills J. Techniques for the measurement of the local myocardial extraction efficiency for inert diffusible contrast agents such as gadopentate dimeglumine. Magn Reson Med. 1993;30(14):332–6.
13. Pereira RS, Prato FS, Sykes J, Wisenberg G. Assessment of myocardial viability using MRI during a constant infusion of Gd-DTPA: further studies at early and late periods of reperfusion. Magn Reson Med. 1999;42(1):60–8.
14. Pereira RS, Prato FS, Wisenberg G, Sykes J. The determination of myocardial viability using Gd-DTPA in a canine model of acute myocardial ischemia and reperfusion. Magn Reson Med. 1996;36:684–93.
15. Pereira RS, Prato FS, Lekx KS, Sykes J, Wisenberg G. Contrast-enhanced MRI for the assessment of myocardial viability after permanent coronary artery occlusion. Magn Reson Med. 2000;44(2):309–16.
16. Pereira RS, Wisenberg G, Prato FS, Yvorchuk K. Clinical assessment of myocardial viability using MRI during a constant infusion of Gd-DTPA. MAGMA. 2000;11(3):104–13.
17. Flacke SJ, Fischer SE, Lorenz CH. Measurement of the gadopentetate dimeglumine partition coefficient in human myocardium in vivo: normal distribution and elevation in acute and chronic infarction. Radiology. 2001;218:703–10.
18. Choi KM, Kim RJ, Gubernikoff G, Vargas JD, Parker M, Judd RM. Transmural extent of acute myocardial infarction predicts long-term improvement in contractile function. Circulation. 2001;104:1101–7.
19. Ricciardi MJ, Wu E, Davidson CJ, Choi KM, Klocke FJ, Bonow RO, Judd RM, Kim RJ. Visualization of discrete microinfarction after percutaneous coronary intervention associated with mild creatine kinase-MB elevation. Circulation. 2001;103(23):2780–3.
20. Wagner A, Mahrholdt H, Holly TA, Elliott MD, Regenfus M, Parker M, Klocke FJ, Bonow RO, Kim RJ, Judd RM. Contrast-enhanced MRI and routine single photon emission computed tomography (SPECT) perfusion imaging for detection of suben-

docardial myocardial infarcts: an imaging study. Lancet. 2003;361(9355):374–9.
21. Wu E, Judd RM, Vargas JD, Klocke FJ, Bonow RO, Kim RJ. Visualisation of presence, location, and transmural extent of healed Q-wave and non-Q-wave myocardial infarction. Lancet. 2001;357(9249):21–8.
22. Kim RJ, Shah DJ, Judd RM. How we perform delayed enhancement imaging. J Cardiovasc Magn Reson Off J Soc Cardiovasc Magn Reson. 2003;5:505–14.
23. Simonetti O, Chung YC, Lee VS, Laub G. Inversion recovery cine trueFISP for optimizing TI in myocardial infarct imaging. Proc Intl Soc Mag Reson Med. 2002;10:2019.
24. Tong CY, Prato FS, Wisenberg G, Lee TY, Carroll E, Sandler D, Wills J, Drost D. Measurement of the extraction efficiency and distribution volume for Gd-DTPA in normal and diseased canine myocardium. Magn Reson Med. 1993;30(3):337–46.
25. Kim RJ, Fieno DS, Parrish TB, Harris K, Chen E, Simonetti O, Bundy J, Finn JP, Klocke FJ, Judd RM. Relationship of MRI delayed contrast enhancement to irreversible injury, infarct age, and contractile function. Circulation. 1999;100:1992–2002.
26. Rogers WJ, Kramer CM, Geskin G, Hu YL, Theobald TM, Vido DA, Petruolo S, Reichek N. Early contrast-enhanced MRI predicts late functional recovery after reperfused myocardial infarction. Circulation. 1999;99(6):744–50.
27. Judd RM, Reeder SB, Atalar E, McVeigh ER, Zerhouni EA. A magnetization-driven gradient echo pulse sequence for the study of myocardial perfusion. Magn Reson Med. 1995;34:276–82.
28. Simonetti OP, Kim RJ, Fieno DS, Hillenbrand HB, Wu E, Bundy JM, Finn JP, Judd RM. An improved MR imaging technique for the visualization of myocardial infarction. Radiology. 2001;218(9):215–23.
29. Judd R, Kim RJ, Wu E, Rafael A, Chen EL, Parker MA, Simonetti O, Klocke FJ, Bonow RO. The use of contrast-enhanced magnetic resonance imaging to identify reversible myocardial dysfunction. N Engl J Med. 2000;343(20):1445–53.
30. Kim D, Lee VS, Srichai MB. Improved visualization of nontransmural scar using slice-selective inversion-recovery delayed contrast-enhanced MRI : a preliminary report. NMR Biomed. 2007;20:121–7.
31. Kellman P, Arai AE, McVeigh ER, Aletras AH. Phase-sensitive inversion recovery for detecting myocardial infarction using gadolinium-delayed hyperenhancement. Magn Reson Med. 2002;47:372–83.
32. Huber AM, Schoenberg SO, Hayes C, Spannagl B, Engelmann MG, Franz WM, Reiser MF. Phase-sensitive inversion-recovery MR imaging in the detection of myocardial infarction. Radiology. 2005;237:854–60.
33. Kühl HP, Papavasiliu TS, Beek AM, Hofman MBM, Heusen NS, van Rossum AC. Myocardial viability: rapid assessment with delayed contrast-enhanced MR imaging with three-dimensional inversion-recovery prepared pulse sequence. Radiology. 2004;230(2):576–82.
34. Bauner KU, Muehling O, Theisen D, Hayes C, Wintersperger BJ, Reiser MF, Huber AM. Assessment of myocardial viability with 3D MRI at 3 T. AJR Am J Roentgenol. 2009;192(6):1645–50.
35. Saranathan M, Rochitte CE, Foo TKF. Fast, three-dimensional free-breathing MR imaging of myocardial infarction: a feasibility study. Magn Reson Med. 2004;51(5):1055–60.
36. Ehman RL, Felmlee JP. Adaptive technique for high-definition MR imaging of moving structures. Radiology. 1989;173:255–63.
37. Wendland M, Arheden H, Saeed M, Higgins CB, Gao DW, Bremerich J, Wyttenbach R, Dae MW. Measurement of the gadopentetate dimeglumine at echo-planar MR imaging to quantify myocardial infarction : comparison with 99m Tc-DTPA autoradiography in rats. Radiology. 1999;211:698–708.
38. Wendland M, Arheden H, Saeed M, Higgins CB, Gao DW, Ursell PC, Bremerich J, Wyttenbach R, Dae MW. Reperfused rat myocardium subjected to various durations of ischemia: estimation of the distribution volume of contrast material with echo-planar MR imaging. Radiology. 2000;215:520–8.
39. Wendland MF, Saeed M, Lauerma K, Derugin N, Mintorovitch J, Cavagna FM, Higgins CB. Alterations in T_1 of normal and reperfused infarcted myocardium after Gd-BOPTA versus GD-DTPA on inversion recovery EPI. Magn Reson Med. 1997;37:448–56.
40. Higgins C, Saeed M, Lund G, Wendland MF, Bremerich J, Weinmann H. Magnetic resonance characterization of the periinfarction zone of reperfused myocardial infarction with necrosis-specific and extracellular contrast media. Circulation. 2001;103:871–6.
41. Oshinski JN, Yang Z, Jones JR, Mata JF, French BA. Imaging time after Gd-DTPA injection is critical in using delayed enhancement to determine infarct size accurately with magnetic resonance imaging. Circulation. 2001;104(23):2838–42.
42. Inoue S, Murakami Y, Ochiai K, Kitamura J, Ishibashi Y, Kawamitsu H, Sugimura K, Shimada T. The contributory role of interstitial water in Gd-DTPA-enhanced MRI in myocardial infarction. J Magn Reson Imaging. 1999;9(2):215–9.
43. Judd RM, Lugo-Olivieri CH, Arai M, Kondo T, Croisille P, Lima JA, Mohan V, Becker LC, Zerhouni EA. Physiological basis of myocardial contrast enhancement in fast magnetic resonance images of 2-day-old reperfused canine infarcts. Circulation. 1995;92:1902–10.
44. Wu KC, Kim RJ, Bluemke DA, Rochitte CE, Zerhouni EA, Becker LC, Lima JA. Quantification and time course of microvascular obstruction by contrast-enhanced echocardiography and magnetic resonance imaging following acute myocardial infarction and reperfusion. J Am Coll Cardiol. 1998;32(6):1756–64.
45. Gerber BL, Rochitte CE, Bluemke DA, Melin JA, Crosille P, Becker LC, Lima JA. Relation between Gd-DTPA contrast enhancement and regional inotropic response in the periphery and center of myocardial infarction. Circulation. 2001;104(9):998–1004.
46. Hillenbrand HB, Kim RJ, Parker MA, Fieno DS, Judd RM. Early assessment of myocardial salvage by contrast-enhanced magnetic resonance imaging. Circulation. 2000;102(14):1678–83.
47. Fieno DS, Kim RJ, Chen E, Lomasney JW, Klocke FJ, Judd RM. Contrast-enhanced magnetic resonance imaging of myocardium at risk: distinction between reversible and irreversible injury throughout infarct healing. J Am Coll Cardiol. 2000;36(3):1985–91.
48. Dendale P, Franken PR, Block P, Pratikakis Y, De Roos A. Contrast enhanced and functional magnetic resonance imaging for the detection of viable myocardium after infarction. Am Heart J. 1998;135:875–80.
49. Ramani K, Judd RM, Holly TA, Parrish TB, Rigolin VH, Parker MA, Callahan C, Fitzgerald SW, Bonow RO, Klocke FJ. Contrast magnetic resonance imaging in the assessment of myocardial viability in patients with stable coronary artery disease and left ventricular dysfunction. Circulation. 1998;98(24):2687–94.
50. Lauerma K, Niemi P, Janatuinen T, Knuuti J, Toivonen L, Aronen HJ. Multimodality MR imaging assessment of myocardial viability: combination of first-pass and late contrast enhancement to wall motion dynamics and comparison with FDG PET—initial experience. Radiology. 2000;217(5):729–36.
51. Klein C, Nekolla SG, Bengel FM, Momose M, Sammer A, Haas F, Schnackenburg B, Delius W, Mudra H, Wolfram D, Schwaiger M. Assessment of myocardial viability with contrast-enhanced magnetic resonance imaging: comparison with positron emission tomography. Circulation. 2002;105(2):162–7.
52. van Voorthuisen A, de Roos A, Doornbos J, van der Wall EE. MR imaging of acute myocardial infarction: value of Gd-DTPA. AJR Am J Roentgenol. 1988;150:531–4.
53. Judd RM, Kim RJ. Imaging time after Gd-DTPA injection is critical in using delayed enhancement to determine infarct size accu-

rately with magnetic resonance imaging. Circulation. 2002;106(2): e6. p. e6; author reply e6, Jul.
54. Lekx K, Prato F, Sykes J, Wisenberg G. The partition coefficient of Gd-DTPA reflects maintained tissue viability in a canine model of chronic significant coronary stenosis. J Cardiovasc Magn Reson. 2004;6(1):33–42.
55. Rehwald WG, Fieno DS, Chen E-L, Kim RJ, Judd RM. Myocardial magnetic resonance imaging contrast agent concentrations after reversible and irreversible ischemic injury. Circulation. 2002;105(2):224–9.
56. Thornhill RE, Prato FS, Pereira RS, Wisenberg G, Sykes J. Examining a canine model of stunned myocardium with Gd-DTPA-enhanced MRI. Magn Reson Med. 2001;45(5): 864–71.
57. Sun Y, Weber KT. Infarct scar: a dynamic tissue. Cardiovasc Res. 2000;46(2):250–6.
58. Thornhill RE, Prato FS, Wisenberg G. The assessment of myocardial viability: a review of current diagnostic imaging approaches. J Cardiovasc Magn Reson. 2002;4(3):381–410.
59. White JA, Patel MR. The role of cardiovascular MRI in heart failure and the cardiomyopathies. Cardiol Clin. 2007;25(1):71–95. vi.
60. Allman KC, Shaw LJ, Hachamovitch R, Udelson JE. Myocardial viability testing and impact of revascularization on prognosis in patients with coronary artery disease and left ventricular dysfunction: a meta-analysis. J Am Coll Cardiol. 2002;39:1151–8.
61. Kubo N, Morimoto S, Hiramitsu S, Uemura A, Kimura K, Shimizu K, Hishida H. Feasibility of diagnosing chronic myocarditis by endomyocardial biopsy. Hear Vessel. 1997;12:167–70.
62. McCrohon JA, Moon JCC, Prasad SK, McKenna WJ, Lorenz CH, Coats AJS, Pennell DJ. Differentiation of heart failure related to dilated cardiomyopathy and coronary artery disease using gadolinium-enhanced cardiovascular magnetic resonance. Circulation. 2003;108(1):54–9.
63. Gulati A, et al. Association of fibrosis with mortality and sudden cardiac death in patients with nonischemic dilated cardiomyopathy. JAMA. 2013;309(9):896–908. PMID 23462786.
64. Libby P. Braunwald's heart disease: a textbook of cardiovascular medicine. 8th ed. Philadelphia: Saunders Company; 2007.
65. Chun EJ, Il Choi S, Jin KN, Kwag HJ, Kim YJ, Choi BW, Lee W, Park JH. Hypertrophic cardiomyopathy: assessment with MR imaging and multidetector CT. Radiogr Rev Publ Radiol Soc N Am Inc. 2010;30:1309–28.
66. Wilson JM, et al. Imaging of myocardial fibrosis in hypertrophic. Texas Heart Inst J. 2002;29(3):176–80.
67. Teraoka K, Hirano M, Ookubo H, Sasaki K, Katsuyama H, Amino M, Abe Y, Yamashina A. Delayed contrast enhancement of MRI in hypertrophic cardiomyopathy. Magn Reson Imaging. 2004;22(2): 155–61.
68. Rubinshtein R, Glockner JF, Ommen SR, Araoz PA, Ackerman MJ, Sorajja P, Bos JM, Tajik AJ, Valeti US, Nishimura RA, Gersh BJ. Characteristics and clinical significance of late gadolinium enhancement by contrast-enhanced magnetic resonance imaging in patients with hypertrophic cardiomyopathy. Circ Heart Fail. 2010;3(1):51–8.
69. Kim RJ, Judd RM. Gadolinium-enhanced magnetic resonance imaging in hypertrophic cardiomyopathy. J Am Coll Cardiol. 2003;41(9):1568–72.
70. Maron MS, Maron BJ, Harrigan C, Buros J, Gibson CM, Olivotto I, Biller L, Lesser JR, Udelson JE, Manning WJ, Appelbaum E. Hypertrophic cardiomyopathy phenotype revisited after 50 years with cardiovascular magnetic resonance. J Am Coll Cardiol. 2009;54(3):220–8.
71. Choudhury L, Mahrholdt H, Wagner A, Choi KM, Elliott MD, Klocke FJ, Bonow RO, Judd RM, Kim RJ. Myocardial scarring in asymptomatic or mildly symptomatic patients with hypertrophic cardiomyopathy. J Am Coll Cardiol. 2002;40(12):2156–64.
72. Moon JC, McKenna WJ, McCrohon JA, Elliott PM, Smith GC, Pennell DJ. Toward clinical risk assessment in hypertrophic cardiomyopathy with gadolinium cardiovascular magnetic resonance. J Am Coll Cardiol. 2003;41(9):1561–7.
73. O'Hanlon R, Grasso A, Roughton M, Moon JC, Clark S, Wage R, Webb J, Kulkarni M, Dawson D, Sulaibeekh L, Chandrasekaran B, Bucciarelli-Ducci C, Pasquale F, Cowie MR, McKenna WJ, Sheppard MN, Elliott PM, Pennell DJ, Prasad SK. Prognostic significance of myocardial fibrosis in hypertrophic cardiomyopathy. J Am Coll Cardiol. 2010;56:431–4.
74. Adabag AS, Maron BJ, Appelbaum E, Harrigan CJ, Buros JL, Gibson CM, Lesser JR, Hanna CA, Udelson JE, Manning WJ, Maron MS. Occurrence and frequency of arrhythmias in hypertrophic cardiomyopathy in relation to delayed enhancement on cardiovascular magnetic resonance. J Am Coll Cardiol. 2008;51(14):1369–74.
75. Kwon DH, Setser RM, Popović ZB, Thamilarasan M, Sola S, Schoenhagen P, Garcia MJ, Flamm SD, Lever HM, Desai MY. Association of myocardial fibrosis, electrocardiography and ventricular tachyarrhythmia in hypertrophic cardiomyopathy: a delayed contrast enhanced MRI study. Int J Cardiovasc Imaging. 2008;24(6):617–25.
76. Leonardi S, Raineri C, De Ferrari GM, Ghio S, Scelsi L, Pasotti M, Tagliani M, Valentini A, Dore R, Raisaro A, Arbustini E. Usefulness of cardiac magnetic resonance in assessing the risk of ventricular arrhythmias and sudden death in patients with hypertrophic cardiomyopathy. Eur Heart J. 2009;30(16): 2003–10.
77. Sen-Chowdhry S, Syrris P, Ward D, Asimaki A, Sevdalis E, McKenna WJ. Clinical and genetic characterization of families with arrhythmogenic right ventricular dysplasia/cardiomyopathy provides novel insights into patterns of disease expression. Circulation. 2007;115:1710–20.
78. Shimada T, Shimada K, Sakane T, Ochiai K, Tsukihashi H, Fukui M, Inoue S, Katoh H, Murakami Y, Ishibashi Y, Maruyama R. Diagnosis of cardiac sarcoidosis and evaluation of the effects of steroid therapy by gadolinium-DTPA-enhanced magnetic resonance imaging. Am J Med. 2001;110:520–7.
79. Marcus FI, McKenna WJ, Sherrill D, Basso C, Bauce B, Bluemke DA, Calkins H, Corrado D, Cox MGPJ, Daubert JP, Fontaine G, Gear K, Hauer R, Nava A, Picard MH, Protonotarios N, Saffitz JE, Sanborn DMY, Steinberg JS, Tandri H, Thiene G, Towbin JA, Tsatsopoulou A, Wichter T, Zareba W. Diagnosis of arrhythmogenic right ventricular cardiomyopathy/dysplasia: proposed modification of the Task Force Criteria. Eur Heart J. 2010;31:806–14.
80. Steckman DA, Schneider PM, Schuller JL, Aleong RG, Nguyen DT, Sinagra G, Vitrella G, Brun F, Cova MA, Pagnan L, Mestroni L, Varosy PD, Sauer WH. Utility of cardiac magnetic resonance imaging to differentiate cardiac sarcoidosis from arrhythmogenic right ventricular cardiomyopathy. Am J Cardiol. 2012;110(4):575–9.
81. Ayyala US, Nair AP, Padilla ML. Cardiac sarcoidosis. Clin Chest Med. 2008;29:493–508. ix.
82. Silverman KJ, Hutchins GM, Bulkley BH. Cardiac sarcoid: a clinicopathologic study of 84 unselected patients with systemic sarcoidosis. Circulation. 1978;58:1204–11.
83. Roberts WC, McAllister HA, Ferrans VJ. Sarcoidosis of the heart. A clinicopathologic study of 35 necropsy patients (group 1) and review of 78 previously described necropsy patients (group 11). Am J Med. 1977;63:86–108.
84. Smedema J-P, Snoep G, van Kroonenburgh MPG, van Geuns R-J, Dassen WRM, Gorgels APM, Crijns HJGM. Evaluation of the accuracy of gadolinium-enhanced cardiovascular magnetic resonance in the diagnosis of cardiac sarcoidosis. J Am Coll Cardiol. 2005;45(10):1683–90.
85. Wu Y-W, Tadamura E, Kanao S, Yamamuro M, Marui A, Komeda M, Toma M, Kimura T, Togashi K. Myocardial viability by

contrast-enhanced cardiovascular magnetic resonance in patients with coronary artery disease: comparison with gated single-photon emission tomography and FDG position emission tomography. Int J Cardiovasc Imaging. 2007;23(6):757–65.
86. Ichinose A, Otani H, Oikawa M, Takase K, Saito H, Shimokawa H, Takahashi S. MRI of cardiac sarcoidosis: basal and subepicardial localization of myocardial lesions and their effect on left ventricular function. AJR Am J Roentgenol. 2008;191:862–9.
87. Patel MR, Cawley PJ, Heitner JF, Klem I, Parker MA, Jaroudi WA, Meine TJ, White JB, Elliott MD, Kim HW, Judd RM, Kim RJ. Detection of myocardial damage in patients with sarcoidosis. Circulation. 2009;120:1969.
88. Hiroe M, Hiraga H, Yuwai K. Guideline for diagnosis of cardiac sarcoidosis: study report on diffuse pulmonary disease from the Japanese Ministry of Health and Welfare. Tokyo: Japanese Ministry of Health and Welfare; 1993. p. 23–4.
89. Angelini A, Calzolari V, Calabrese F, Boffa GM, Maddalena F, Chioin R, Thiene G. Myocarditis mimicking acute myocardial infarction: role of endomyocardial biopsy in the differential diagnosis. Heart. 2000;84:245–50.
90. Mahrholdt H, Goedecke C, Wagner A, Meinhardt G, Athanasiadis A, Vogelsberg H, Fritz P, Klingel K, Kandolf R, Sechtem U. Cardiovascular magnetic resonance assessment of human myocarditis: a comparison to histology and molecular pathology. Circulation. 2004;109(10):1250–8.
91. Friedrich MG, Strohm O, Schulz-Menger J, Marciniak H, Luft FC, Dietz R. Contrast media-enhanced magnetic resonance imaging visualizes myocardial changes in the course of viral myocarditis. Circulation. 1998;97:1802–9.
92. Shah KB, Inoue Y, Mehra MR. Amyloidosis and the heart: a comprehensive review. Arch Intern Med. 2006;166:1805–13.
93. Duston MA, Skinner M, Shirahama T, Cohen AS. Diagnosis of amyloidosis by abdominal fat aspiration. Analysis of four years' experience. Am J Med. 1987;82:412–4.
94. Maceira AM, Joshi J, Prasad SK, Moon JC, Perugini E, Harding I, Sheppard MN, Poole-Wilson PA, Hawkins PN, Pennell DJ. Cardiovascular magnetic resonance in cardiac amyloidosis. Circulation. 2005;111(2):186–93.
95. Vogelsberg H, Mahrholdt H, Deluigi CC, Yilmaz A, Kispert EM, Greulich S, Klingel K, Kandolf R, Sechtem U. Cardiovascular magnetic resonance in clinically suspected cardiac amyloidosis: noninvasive imaging compared to endomyocardial biopsy. J Am Coll Cardiol. 2008;51:1022–30.
96. Syed IS, Glockner JF, Feng D, Araoz PA, Martinez MW, Edwards WD, Gertz MA, Dispenzieri A, Oh JK, Bellavia D, Tajik AJ, Grogan M. Role of cardiac magnetic resonance imaging in the detection of cardiac amyloidosis. JACC Cardiovasc Imaging. 2010;3:155–64.
97. Perugini E, Rapezzi C, Piva T, Leone O, Bacchi-Reggiani L, Riva L, Salvi F, Lovato L, Branzi A, Fattori R. Non-invasive evaluation of the myocardial substrate of cardiac amyloidosis by gadolinium cardiac magnetic resonance. Heart. 2006;92:343–9.
98. Srichai MB, Junor C, Rodriguez LL, Stillman AE, Grimm RA, Lieber ML, Weaver JA, Smedira NG, White RD. Clinical, imaging, and pathological characteristics of left ventricular thrombus: a comparison of contrast-enhanced magnetic resonance imaging, transthoracic echocardiography, and transesophageal echocardiography with surgical or pathological validation. Am Heart J. 2006;152:75–84.
99. Weinsaft JW, Kim HW, Shah DJ, Klem I, Crowley AL, Brosnan R, James OG, Patel MR, Heitner J, Parker M, Velazquez EJ, Steenbergen C, Judd RM, Kim RJ. Detection of left ventricular thrombus by delayed-enhancement cardiovascular magnetic resonance prevalence and markers in patients with systolic dysfunction. J Am Coll Cardiol. 2008;52:148–57.
100. Peters DC, Wylie JV, Hauser TH, Kissinger KV, Josephson ME, Manning WJ. Detection of pulmonary vein and left atrial scar after catheter ablation with three-dimensional navigator-gated delayed enhancement MR imaging: methods: results: conclusion. Radiology. 2007;243(3):690–5.
101. Oakes RS, Badger TJ, Kholmovski EG, Akoum N, Burgon NS, Fish EN, Blauer JJE, Rao SN, DiBella EVR, Segerson NM, Daccarett M, Windfelder J, McGann CJ, Parker D, MacLeod RS, Marrouche NF. Detection and quantification of left atrial structural remodeling with delayed-enhancement magnetic resonance imaging in patients with atrial fibrillation. Circulation. 2009;119(13):1758–67.
102. Kramer CM, Barkhausen J, Flamm SD, Kim RJ, Nagel E. Standardized cardiovascular magnetic resonance imaging (CMR) protocols, society for cardiovascular magnetic resonance: board of trustees task force on standardized protocols. J Cardiovasc Magn Reson. 2008;10:1–10.
103. Amado LC, Gerber BL, Gupta SN, Rettmann DW, Szarf G, Schock R, Nasir K, Kraitchman DL, Lima JC. Accurate and objective infarct sizing by contrast-enhanced magnetic resonance imaging in a canine myocardial infarction model. J Am Coll Cardiol. 2004;44(12):2383–9.
104. Flett AS, Hasleton J, Cook C, Hausenloy D, Quarta G, Ariti C, Muthurangu V, Moon JC. Evaluation of techniques for the quantification of myocardial scar of differing etiology using cardiac magnetic resonance. JACC Cardiovasc Imaging. 2011;4(2):150–6.